Transactions of the Materials Research Society of Japan 33[2] 339-344 (2008)

Chemical state analysis of implanted nitrogen in visible-light response TiO_2 photocatalyst

Tomoko Yoshida and Shunsuke Muto
Division of Quantum Science and Energy Engineering, Department of Materials, Physics and Energy Engineering, Graduate School of Engineering, Nagoya University, Furo-cho, Chikusa-ku, Nagoya 464-8603, JAPAN

Fax: 81-52-789-5137, e-mail: tyoshida@nucl.nagoya-u.ac.jp

It was found that nitrogen-doped TiO_2 revealed significant improvement in high photocatalytic reactivity under visible-light [Asahi *et al*, *Science* **293**, 269-271 (2001)]. To investigate the optimal local concentration of doped nitrogen for visible-light response, N^+-implanted TiO_2 samples were examined by means of X-ray absorption near edge structure (XANES) and electron energy loss spectroscopy (EELS). Depth-resolved nitrogen K-edge EELS revealed two types of chemical state of nitrogen, depending on the concentration, consistent with the XANES results. We found that the local nitrogen concentration effective for visible-light response was approximately less than 1 at%. Further, we visualized the spatial distributions of the different chemical states of nitrogen by energy-filtering TEM (FETEM). It was also found that the photocatalytic activity was offset by the coexisting inactive state.

Keywords: photocatalyst, ion implantation, XANES, EELS, EFTEM

1. INTRODUCTION

In the field of catalytic chemistry, a specific function in a solid catalyst crucially depends on the chemical state of a specific active component (active site). In this context X-ray absorption fine structure (XAFS) and electron energy loss spectroscopy (EELS) are expected as one of the most powerful techniques for chemical state analysis of the active site, because they provide information on the local structure and electronic states around the specific element of interest. However, in a solid catalyst, different chemical states of the same elements generally coexist, and thus the XAFS and EELS associated with those chemical states often overlap each other, inseparable to the single spectrum of each state.

The nitrogen (N) doped TiO_2 has been attracting much attention due to its visible-light response to natural solar light [1]. The doped N has been regarded as the catalytically active site generating the visible-light response in TiO_2, since the optical absorbance in the visible-light region evolved with increasing N concentration. However, as reported by previous works, the absorbance was not always linearly proportional to the photocatalytic activity [2,3], and it is thus important to understand the chemical environment and the optimum concentration of the dopant.

The purpose of the present study is to examine depth dependence of the local chemical states of N injected into TiO_2 photocatalyst by means of a sophisticated combination of XAFS and EELS, particularly introducing current mathematical treatments to the EELS and energy-filtering TEM spectrum imaging (EFTEM-SI). In an effort to investigate those factors, we applied an ion implantation technique for N doping, because it enables to the depth and concentration of the implants to be easily controlled by changing their energy and fluence.

2. EXPERIMENTAL

2.1 Sample preparation

The samples used in this study were TiO_2 (1 0 0) single crystals (5 x 5 x 0.5 mm^3), supplied by Furuuchi Kagaku, Japan. Mass analyzed 100 keV N_2^+ ions (50 keV/ N^+ ion) were injected into the samples at room temperature, perpendicular to the sample surface. The N^+ fluence ranged from 1 to 5 x 10^{21} m^{-2}. A Monte Carlo calculation (SRIM code)[4] indicated that the implanted N atoms were distributed up to ~180 nm, peaking around 90 nm in depth from the surface. After the ion implantation, parts of the samples were heat-treated at 573 K for two hours in air.

Cross-section samples for observing the depth distributions of N-related electronic structures were prepared by the standard sample preparation procedures for semiconductors and ceramics.

2.2 Photocatalytic response test

A typical photocatalytic experiment consisted of placing the N^+-implanted sample in 0.5 ml of aqueous methylene-blue (MB) solution (9.8 μmol/L) and subsequent exposure to visible-light using a 15 W Xe lamp with a cut filter for $\lambda >$ 430 nm. The light absorbance at λ = 664 nm after exposure for 2 hours was measured to estimate the photocatalytic activity of the samples.

2.3 XANES measurements

N K-edge absorption near edge structure (XANES) of the N^+-implanted TiO_2 samples were measured at the

BL-8B1 station of UVSOR-II at the Institute for Molecular Science, Okazaki, Japan. Data were recorded at room temperature in the total electron yield mode, and the X-ray energy dependence of the Auger electron yield was monitored [5]. Considering the escape depth of the Auger electrons, the spectra probe the sample from the surface up to a few nanometers in depth.

2.4 Depth-resolved EELS (DREELS)[6]

EEL spectra were recorded with a Gatan ENFINA 1000 spectrometer attached to a JEM200CX TEM operated at 200 kV. The detecting system consists of a fiber-coupled YAG scintillater combined with a CCD of 1340 x 100 pixels.

The DREELS were recorded in a manner similar to a spatially resolved EELS (SREELS) technique [7], but extending its capability for detecting trace elements [6].

The intensity-corrected image still suffers spectrum blurring, not only due to the instrumental point-spread function (PSF) in the dispersion direction but also due to the beam spread (defocus) in the cross-dispersion direction. These effects were dramatically improved and statistical noise was removed by spectrum deconvolution, using the PIXON method, the principle and practical examples of which are given in ref. [8-10].

2.5 Electronic structure-resolved EFTEM by multivariate analysis [6]

EFTEM images were acquired with a JEOL-JEM2100F microscope operated at 200 kV, equipped with a Gatan imaging filter (GIF-TRIDIEM, 2k x 2k CCD). The EFTEM-spectrum imaging (EFTEM-SI) method applied to the energy loss near edge structure (ELNES) of the N K-edge: 20 EFTEM images were collected by scanning an energy slit of 2 eV a width from 380 eV to 420 eV on the energy-loss axis at the interval of 2 eV [11]. Spatial drifts of the sample on the images were corrected by the cross-correlation method. A set of image intensities taken out of a specific point and aligned in order of energy-loss through the entire image stack represent the EEL spectrum at that position with an energy dispersion of 2 eV/channel. The pre-edge background was then modeled by a power-law for the intensities between 380-390 eV, and then subtracted from the images to obtain EFTEM images of the N K-edge ELNES, using the functions on DigitalMicrograph™.

The EEL spectrum at each position is supposed to be a linear combination of multiple ELNES features with different weights, each corresponding to a different chemical state of the implanted N, depending on the position. We hence applied a self-modeling curve resolution (SMCR) technique to decompose the set of spectral profiles into individual pure components without reference spectra. We adopted a fast, accurate and robust algorithm, called the modified alternating least-squares (MALS) method [12].

3. RESULTS

3.1 Photocatalytic reactivity under visible-light irradiation

Fig. 1 shows optical absorption spectra of the

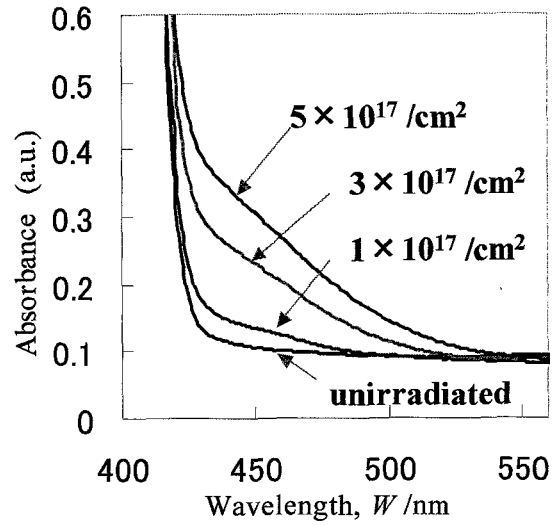

Fig. 1 Optical absorption spectra of N^+-implanted samples.

N^+-implanted samples. The absorbance in the visible-light region from 420 nm to 550 nm increased with the N^+ fluence, suggesting the generation of visible-light responsiveness.

Fig. 2 shows the N^+ fluence dependences of the photocatalytic activity under visible-light irradiation for as-implanted and 573 K annealed samples. The photocatalytic activity reached its maximum at the fluence of 3×10^{21} m^{-2} and then decreased with the fluence. The sample N^+-implanted at 5×10^{21} m^{-2} followed by heat-treatment at 573 K was almost photocatalytically inactive under visible-light irradiation. The visible-light responsiveness is hence not directly connected with the photo-absorbance, which is consistent with the previous reports [2,3].

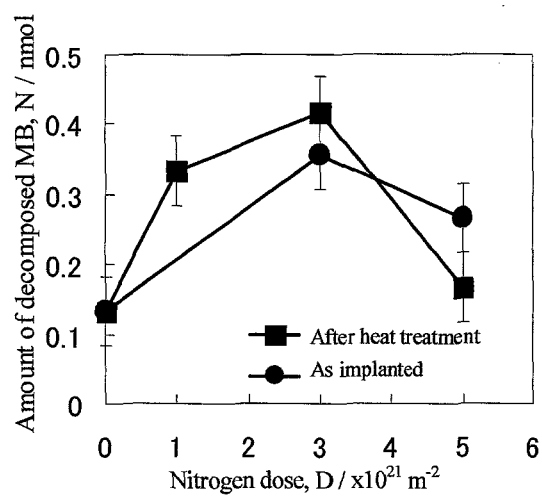

Fig. 2 Amount of decomposed MB after visible-light irradiation for 2 h as a function of N^+ fluence.

3.2 N K-edge XANES

Fig. 3 shows N K-edge XANES spectra of the N^+-implanted TiO_2 samples and a TiN powder for reference. Common XANES features in (a) and (b) suggest that N in the sample N^+-implanted at 3 x 10^{21} m^{-2} (photocatalytically most active) is in a chemical environment similar to that in TiN. More thorough observation suggested that double-peak around 400 eV in (b) shifted to the lower energy side compared with that of TiN, which was well reproduced by the theoretical prediction, using FEFF code [13] for the model where N occupies one of the oxygen sites (O sites) of TiO_2, as suggested in ref. [1]. On the other hand, the XANES spectrum of the sample N^+-implanted at 5 x 10^{21} m^{-2} followed by heat-treatment (almost inactive to visible-light) shows a distinct single peak around 401 eV. This peak was empirically attributable to the formation of molecular species such as N–O and/or N–N bonds near the surface [14].

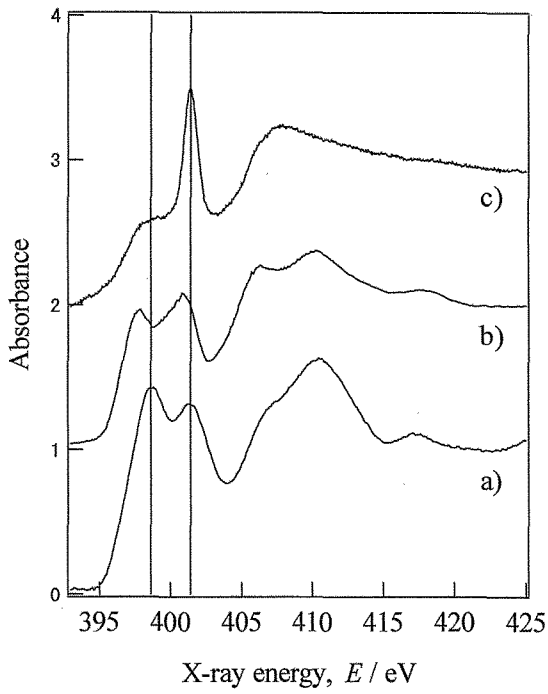

Fig. 3 N K-edge XANES spectra of a TiN(a), N^+-implanted at 3 x 10^{21} m^{-2}(b) and 5 x 10^{21} m^{-2} followed by heating at 573 K for 2 h(c).

3.3 DREELS

Fig. 4 shows extracted profiles of the N K-edge DREELS of the samples N^+-implanted at 3 x 10^{21} m^{-2}. The double-peak structure around 398-401 eV was again observed near the surface region, and the distinct single peak around 401 eV gradually grows with increasing depth, which reflects the different chemical states of N, presumably depending on the local N concentration.

The double-peak structure near the surface

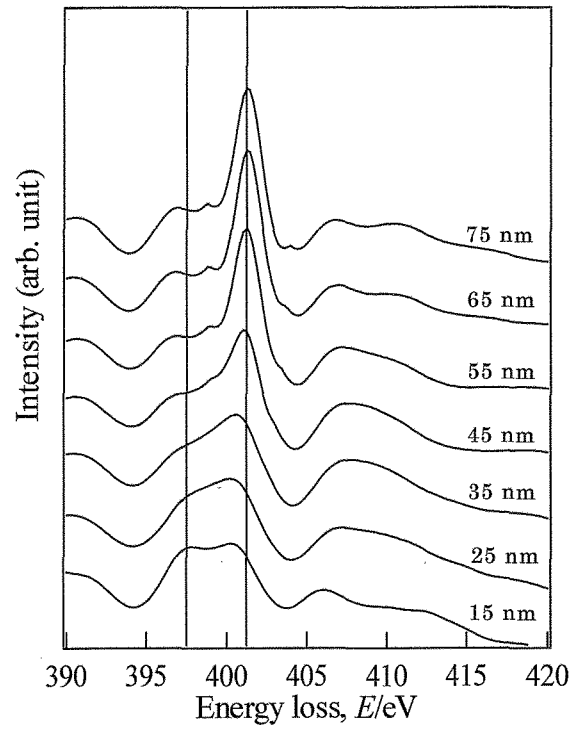

Fig. 4 N K-edge DREELS of photocatalytically active sample, N^+-implanted at 3 x 10^{21} m^{-2}. The corresponding depth from the surface is shown for each spectrum.

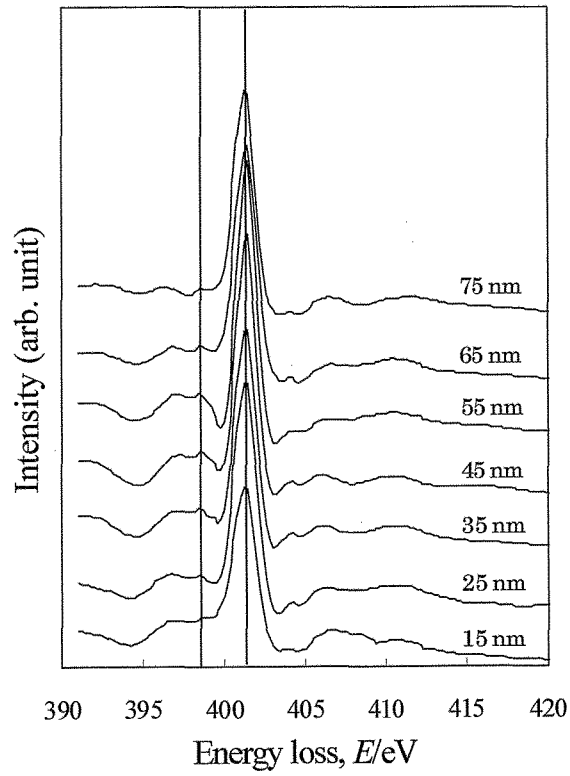

Fig. 5 Depth-resolved N-*K* ELNES of the photocatalytic inactive sample (N^+-implanted at 5 x 10^{21} m^{-2} followed by heating at 573 K for 2 hours)

region is in good agreement with the XANES spectrum of the same sample, indicating that N atoms replacing the O sites in TiO_2 are dominant up to about 25 nm from the surface. On the other hand the single peak around 401 eV for the deeper regions was observed both in XANES (Fig. 3, c) and ELNES over the entire implanted region of the catalytically inactive sample (the sample implanted at the fluence of 5 x 10^{21} m^{-2}, followed by heat-treatment at 573 K) (Fig. 5). Considering that the photocatalytic reactions predominate near the surface, the visible-light responsive property should be closely related to the double-peak structure in the XANES/ELNES. Thus, we confirmed that substitutional N at O sites is essential for visible-light responsive photocatalytic activity.

3.4 Mapping depth distributions of different chemical states of N by multivariate analysis

Since there were at least two kinds of chemical states of N in the N^+-implanted TiO_2, we attempted 'chemical state mapping' by applying the SMCR technique. The area consisting of 100 x 150 pixels was used, and thus 15000 spectra were utilized for the spectral decomposition. In the present case, the number of components was assumed to be two. 200 iterative least-square fitting yielded a sufficiently converged result. The resolved spectra for the sample N^+-implanted at 3 x 10^{21} m^{-2} are shown in Fig. 6(a). Each resolved component well reproduces the corresponding feature of the XANES/ELNES spectra, although component #2 (related to visible-light responsive area) accompanies by a rather high level of post-edge background. This is partly because of the multiple-loss due to the sample thickness of nearly 0.6λ (λ: mean free path for inelastic scattering) and partly because of inappropriate modeling for the pre-edge background. We attempted the procedure by assuming three components, which yielded no physically significant result.

The depth distributions (SI) of the components #1 and #2 are shown in Figs. 6(b) and (c). The grayscale of each image was calibrated such that it reflects the approximate relative concentration of each component. Note that the chemical state of component #1, namely catalytic inactive N is localized over the depth regions deeper than 40 nm, whereas component #2, namely catalytic active N is distributed over the entire implanted region. The local concentration of doped N, most effective for visible-light response, was estimated from the average N concentration up to 30 nm from the surface to be approximately less than 1 at%.

We also applied the same analysis to the photocatalytically inactive sample. The resolved spectra showed essentially similar shapes to those for photocatalytically active sample (Fig. 7(a)), which guarantees the reliability of the present spectral decomposition. In addition, as shown in Figs. 7(b) and (c), the fraction of the chemical

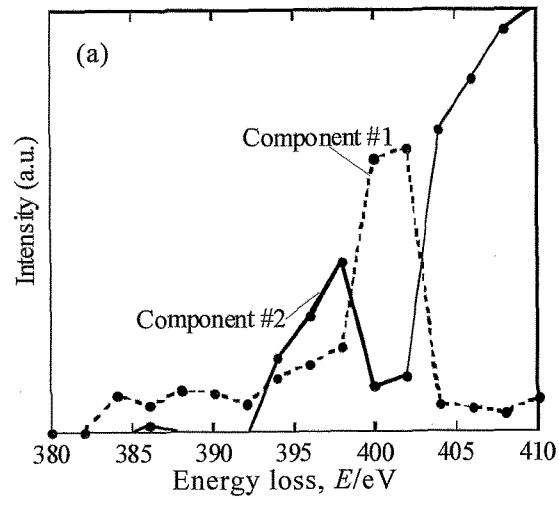

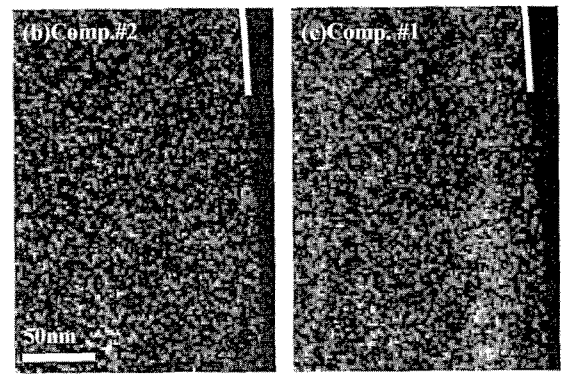

Fig. 6 Resolved spectra (a) and 2D plot of relative concentration for each pure component (b,c) of photocatalytically active sample by SMCR processing. The surface is indicated by solid line in (b) and (c).

state of component #1 increased at the very surface region, whereas component #2 was still distributed quite homogeneously over the entire implanted depth. It thus follows that even in the photocatalytically inactive sample, N atoms replacing the O sites in TiO_2 are distributed at ~1 at% over the implanted regions. Considering that heat treatment at 573 K slightly improved the photocatalytic activity for the sample of 3 x 10^{21} N^+m^{-2}, whereas it slightly deteriorated the activity for samples of higher fluence, the inactive species act as centers that can cancel out the visible-light response created by the substitutional N.

4. DISCISSION

4.1 Comparison with recent theoretical calculations

Asahi and Morikawa systematically discussed the stability of the various N-species in TiO_2 in terms of the first principle theoretical calculation [15]: substitutional N- ($(N)_O$), interstitial N- ($(N)_i$), substitutional NO- ($(NO)_O$), substitutional NO_2- ($(NO_2)_O$) and interstitial NO-doping ($(NO)_i$). The estimated N 1s binding

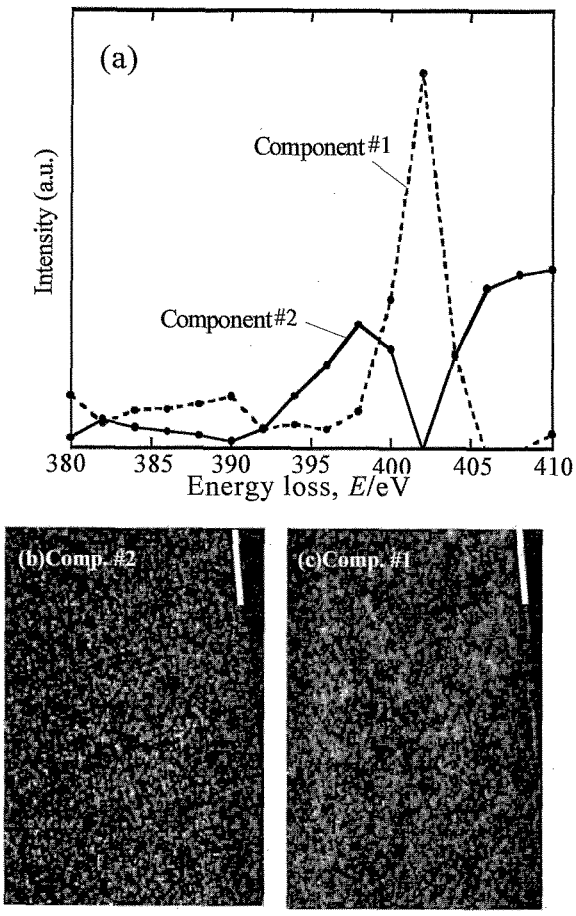

Fig. 7 Resolved spectra (a) and 2D plot of relative concentration for each pure component (b,c) of photocatalytically inactive sample by SMCR processing.

energies were 365.7, 397.7, 398.1, 399.8 and 399.9 eV within the accuracies of 0.10-0.17 eV for each model, respectively. These values can be compared with the experimental edge-onset energies of N K-edge XANES and ELNES in the present study. The double peak of the photocatalytically active component and the single peak of the inactive one can be thus assigned to $(N)_O$ and $(NO_2)_O$ and/or $(NO)_i$, respectively, which was consistent with our assignment. They also claimed that the $(NO_2)_O$ and $(NO)_i$ species accompany by a large distortion of the TiO_2 lattice, so that these species are expected to be found mostly at the surface or in the voids. The present N-doping by the energetic ion injection technique must introduce a lot of defects and may promote the formation of the $(NO_2)_O$ and $(NO)_i$ species associated with the subsequent thermal anneal.

They also showed the calculated projected densities of states (DOS) into the doped anion sites for the species: the newly formed energy levels associated with the N-doping are located at the top of the valence band for $(N)_O$, but isolated in the band gap for the other species. In particular, the defect levels just below the conduction band for the $(NO_2)_O$ and $(NO)_i$ species may act as recombination centers for the photo-generated electrons. This effect should significantly reduce the photocatalytic reactions, as experimentally suggested.

4.2 Radiation induced defects

Energetic ion injection inevitably introduces radiation damages, which may affect the photocatalytic activity. We examined the near surface structure by high-resolution TEM (HRTEM) and fast Fourier transform (FFT) of the images.

A cross-sectional HRTEM image of the as-implanted sample (3 x 10^{21} m^{-2}, highest activity) near the surface and its FFT power spectrum are shown in Figs. 8(a) and (b). The original rutile structure is still maintained, though the (100) spacing parallel to the surface suffers modulations, as shown in the FFT, in which sharp streaks extend normal to the (100) planes. This modulation could be ascribed to the preferential displacements of oxygen atoms (lighter element). Theoretical total DOS of TiO_2 including an oxygen vacancy $((V)_O)$ [15] exhibits no significant change around the valence band maximum (VBM). Hence the radiation damages likely exerted little influence on the photocatalytic activity for visible-light illumination.

An HRTEM image of the photocatalytically inactive sample (N^+-implanted at 5 x 10^{21} m^{-2} followed by heating at 573 K for 2 hours) and FFT power spectra from the corresponding areas are shown in Figs. 9(a)-(c), respectively. Stacking faults and polycrystalline structures are partly observed, indicating thermal recovery from highly defective structures. Furthermore, the framed area, b in Fig. 9(a) and its FFT in (b) show that the structure of the area is better explained by a mixture of rutile and anataze structures. This is consistent with the previous report [16] that amorphous TiO_2 tends to be recrystallized into anataze structure. The present experimental results suggested that thermal recovery does not affect the photocatalytic activity very much for visible-light because the activity almost vanished for the sample N^+-implanted at 5 x 10^{21} m^{-2} after the thermal annealing.

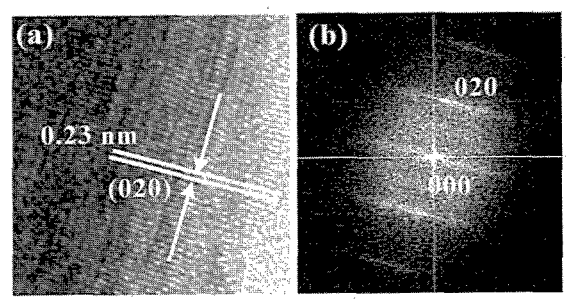

Fig. 8 HRTEM image near the surface of photo-catalytically active sample (N^+-implanted at 3 x 10^{21} m^{-2}) (a) and its FFT power spectrum (b). The surface in (a) is located at the lower right corner.

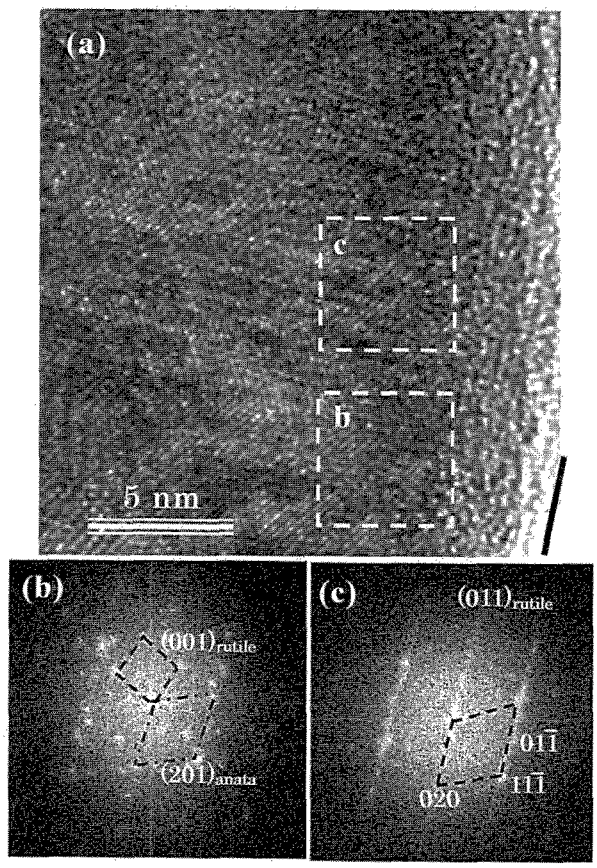

Fig. 9 (a) HRTEM image of the photocatalytically inactive sample (N^+-implanted at 5 x 10^{21} m^{-2} followed by heating at 573 K for 2 hours) and (b) FFT power spectra from the framed areas shown in (a). The surface is indicated by solid line.

5. SUMMARY

The local chemical state and most effective concentration of nitrogen (N) for highly-active visible-light responsive photocatalysis was investigated for N^+-implanted TiO_2 samples, using XANES, and TEM-ELNES techniques. As a result, two chemical states of N, depending on the local N concentration, were identified. One was a state in which photocatalytically active N atoms replace the oxgen sites in TiO_2 and the other was the inactive state in which the N–O and/or N–N species formed at regions of higher N concentrations. The most effective local N concentration for photocatalysis was estimated from the DREELS results to be approximately less than 1 at%. Furthermore, the depth distributions of the two N species revealed for highest active sample that the catalytically active N species were distributed over the entire implanted region, whereas the inactive N species were in the region of higher N concentration. This analysis also suggested for the inactive sample that the inactive N species existing near the surface cancel out the visible-light response created by the substitutional N atoms.

ACKNOWLEDGEMENTS

We are very grateful to Mrs. E. Okunishi, N. Endo and T. Oikawa at Akishima works of JEOL Ltd. for kindly conducting FETEM-SI, essential for the present study. The present work was supported in part by a Grant-in-Aid for Scientific Research (KAKENHI) in Priority Area (#474) "Atomic Scale Modification" and "Kiban-Kenkyu A" from MEXT, Japan.

REFERENCES

[1] R. Asahi, T. Morikawa, T. Ohwaki, K. Aoki and Y. Taga, *Science* **293**, 269-271 (2001).

[2] H Irie, Y. Watanabe and K. Hashimoto, *J. Phys. Chem.* B, **107**, 5483-5486 (2003).

[3] Y. Nosaka, M. Matsushita, J. Nishino and A. Y. Nosaka: *Sci. Tech. Adv. Mater.*, **6**, 143-148 (2005).

[4] http://www.srim.org/SRIM/SRIM2003.htm

[5] A. Erbil, G. S. Cargil, R. Frahm, R. F. Boehme, *Phys. Rev.* B, **37**, 2450-2464 (1988).

[6] T. Yoshida, S. Muto and J. Wakabayashi, *Mater. Trans.* **48**, 2580-2584 (2007).

[7] K. Kimoto, T. Sekiguchi and T. Aoyama: *J. Electron Microsc.* **46**, 369–374 (1997).

[8] P. K. Pina and R. C. Putter: *Astr. Soc. Pac,* **105**, 630-637 (1993).

[9] S. Muto, R. C. Puetter and K. Tatsumi, *J. Elect. Micros.* **55**, 215-223 (2006).

[10] S. Muto, K. Tatsumi, R. C. Puetter, T. Yoshida, Y. Yamamoto and Y. Sasano: *J. Elect. Micros.* **55**, 225-230 (2006).

[11] J. M. Martin, B. Vacher, L. Ponsonnet and V. Dupuis: *Ultramicroscopy*, **65**, 229-238 (1996).

[12] J-H. Wang, P. K. Hopke, T. M. Hancewicz, S. L. Zhang, *Anal. Chim. Acta* **476**, 93-109 (2003).

[13] A. L. Ankudinov, B. Ravel, J. J. Rehr, and S. D. Conradson, *Phys. Rev.* B **58**, 7565-7576 (1998).

[14] J. Stöhr and R. Jaeger, *Phys. Rev.* B, **26**, 4111-4131 (1982)

[15] R. Asahi and T. Morikawa, *Chem. Phys.* **339**, 57-63 (2007).

[16] T. Nakamura, T. Ichitsubo, E. Matsubara, A. Muramatsu, N. Sato and H. Takahashi, *Acta Materialia*, **53**, 323-329 (2005).

(Recieved September 5, 2007 ; Accepted December 22, 2007)